(μ-Oxo)bis(μ-carboxylato)bis(2,2′-bipyridyl)bis(X)diiron(III) Complexes, X = NCS^-, $NCSe^-$, and N_3^-: Synthetic Models of Pseudohalide Derivatives of Carboxylate-Bridged Diiron Proteins

Tadashi J. Mizoguchi and Stephen J. Lippard*

Department of Chemistry, Massachusetts Institute of Technology, Cambridge, Massachusetts 02139

Received April 4, 1997[⊗]

The neutral (μ-oxo)bis(μ-carboxylato)diiron(III) complexes [Fe_2O(μ-XDK)(bpy)$_2$(NCS)$_2$] (**1**), [Fe_2O(μ-XDK)(bpy)$_2$-(^{15}NCS)$_2$] (**1a**), [Fe_2O(μ-XDK)(bpy)$_2$(NCSe)$_2$] (**2**), [Fe_2O(μ-XDK)(bpy)$_2$(N_3)$_2$] (**3**), and [Fe_2O(μ-XDK)(bpy)$_2$-(^{15}NNN)$_2$] (**3a**), where XDK is the doubly deprotonated form of *m*-xylylenediamine bis(Kemp's triacid imide) and bpy is 2,2′-bipyridyl, have been synthesized. The octahedrally coordinated iron centers are triply bridged by an oxo group and the two carboxylate groups of XDK. In the X-ray crystal structures of **1** and **2**, the diiron centers have C_2 symmetry, whereas in **3** the coordinated azide ligands are also anti with respect to the Fe−O−Fe plane but in different rotational conformations with respect to the Fe−N_3 bond. The optical spectra of these highly colored compounds are characterized by broad ligand-field bands centered ∼650 nm and a more intense combination of ligand-field and ligand-to-metal charge-transfer bands between 350 and 500 nm. Compounds **1**−**3** exhibit intense IR bands (∼2050 cm^{-1}) which are characteristic of terminally bound isothiocyanate, isoselenocyanate, and azide ligands, respectively. These bands shift to lower energies upon substitution with $^{15}NCS^-$ in **1a** ($\Delta\nu$ = 24 cm^{-1}) and $^{15}NNN^-$ in **3a** ($\Delta\nu$ = 8 cm^{-1}), and the failure of the latter to reveal two resolved features indicates a need for caution in interpreting analogous data from isotopically substituted protein adducts. Resonance Raman experiments on **1**−**3** revealed bands (∼520 cm^{-1}) attributable to the symmetric FeOFe stretching frequency. The Mössbauer spectra of **1**−**3** at 77 K display symmetric quadrupole doublets with isomer shifts (∼0.5 mm s^{-1}) and quadrupole splittings (∼1.7 mm s^{-1}) typical of (μ-oxo)diiron(III) compounds. Crystal data: **1**·2C_6H_6, monoclinic, $P2_1/n$, a = 19.6692(2) Å, b = 14.3069(1) Å, c = 22.6502(3) Å, β = 96.922(1)°, V = 6327.4(1) Å^3, Z = 4, T = −90 °C; **2**·2C_6H_6, monoclinic, $C2/c$, a = 22.6834(3) Å, b = 14.4315(2) Å, c = 19.7013(4) Å, β = 97.837(1)°, V = 6389.1(2) Å^3, Z = 4, T = −85 °C; **3**·CH_2Cl_2·$C_6H_3(CH_3)_3$, triclinic, $P\bar{1}$, a = 12.1645(2) Å, b = 14.9196(3) Å, c = 18.0690(3) Å, α = 79.688(1)°, β = 78.611(1)°, γ = 83.453(1)°, V = 3152.3(1) Å^3, Z = 2, T = −85 °C.

Introduction

Proteins containing carboxylate-bridged diiron active sites perform a variety of biochemical functions.[1] For example, hemerythrin (Hr) binds dioxygen reversibly; the R2 subunit of ribonucleotide reductase and the soluble form of methane monooxygenase consume dioxygen to generate a tyrosyl radical and to convert methane to methanol, respectively; and mammalian purple acid phosphatase catalyzes phosphate ester hydrolysis. It is of interest not only to understand how these non-heme diiron proteins effect their respective chemical transformations but also to determine what factors direct the reactivity of their metallocenters to achieve a particular function. We continue to address these issues through the synthesis and study of small inorganic model compounds that are designed to mimic aspects of the active-site properties of these metalloproteins.[2−6]

The doubly deprotonated form of *m*-xylylenediamine bis(Kemp's triacid imide) (XDK)[7] has proved to be a useful ligand in the synthesis of model compounds of proteins with carboxylate-bridged dimetallic active sites. X-ray crystallographic analyses of XDK complexes with two identical[4,6,8] as well as different[9] metal ions have been reported. These investigations reveal a doubly bridging coordination mode in which the two

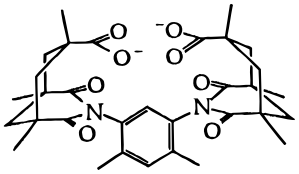

XDK

oxygen atoms from each of the convergent carboxylate groups of XDK link the two metal ions. Furthermore, owing to the conformational constraints imposed by the structure of the XDK ligand, the metal ions often lie above the plane of the nearly

[⊗] Abstract published in *Advance ACS Abstracts,* September 1, 1997.

(1) For reviews, see: (a) Wallar, B. J.; Lipscomb, J. D. *Chem. Rev.* **1996**, *96*, 2625−2657. (b) Nordlund, P.; Eklund, H. *Curr. Opin. Struct. Biol.* **1995**, *5*, 758−766. (c) Feig, A. L.; Lippard, S. J. *Chem. Rev.* **1994**, *94*, 759−805. (d) Howard, J. B.; Rees, D. C. *Adv. Protein Chem.* **1991**, *42*, 199−280.

(2) (a) Armstrong, W. H.; Spool, A.; Papaefthymiou, G. C.; Frankel, R. B.; Lippard, S. J. *J. Am. Chem. Soc.* **1984**, *106*, 3653−3667. (b) Taft, K. L.; Masschelein, A.; Liu, S.; Lippard, S. J.; Garfinkel-Shweky, D.; Bino, A. *Inorg. Chim. Acta* **1992**, *198*−200, 627−631. (c) Goldberg, D. P.; Koulougliotis, D.; Brudwig, G. W.; Lippard, S. J. *J. Am. Chem. Soc.* **1995**, *117*, 3134−3144. (d) Kim, K.; Lippard, S. J. *J. Am. Chem. Soc.* **1996**, *118*, 4914−4915. (e) Feig, A. L.; Masschelein, A.; Bakac, A.; Lippard, S. J. *J. Am. Chem. Soc.* **1997**, *119*, 334−342.

(3) Beer, R. H.; Tolman, W. B.; Bott, S. G.; Lippard, S. J. *Inorg. Chem.* **1991**, *30*, 2082−2092.

(4) Watton, S. P.; Masschelein, A.; Rebek, J., Jr.; Lippard, S. J. *J. Am. Chem. Soc.* **1994**, *116*, 5196−5205.

(5) Feig, A. L.; Bautista, M. T.; Lippard, S. J. *Inorg. Chem.* **1996**, *35*, 6892−6898.

(6) Herold, S.; Lippard, S. J. *J. Am. Chem. Soc.* **1997**, *119*, 145−156.

(7) (a) Rebek, J., Jr.; Marshall, L.; Wolak, R.; Parris, K.; Killoran, M.; Askew, B.; Nemeth, D.; Islam, N. *J. Am. Chem. Soc.* **1985**, *107*, 7476−7481. (b) Marshall, L.; Parris, K.; Rebek, J., Jr.; Luis, S. V.; Burguete, M. I. *J. Am. Chem. Soc.* **1988**, *110*, 5192−5193.

S0020-1669(97)00397-2 CCC: $14.00

coplanar carboxylate groups in the presence of additional bridging ligands. Diiron(III) complexes of XDK have been prepared containing a third bridge provided by an oxo group,[4] resulting in a structure very similar to the active sites of the met, azidomet, and oxy forms of Hr.[10]

Early insights into the structure−function relationship in Hr derived from studying the spectroscopic properties of its pseudohalide-bound adducts. Crystallographic investigations later revealed that metazido- and oxyHr bind their respective ligands in nearly the same fashion.[10] Pseudohalides continue to be used as stable probes of the active-site structures of non-heme diiron proteins. Recent examples include studies of the azide adducts of the stearoyl−acyl carrier protein Δ^9 desaturase (Δ9D)[11] and recombinant wild-type and mutant forms of the dioxygen-binding protein myohemerythrin.[12] Diiron model compounds containing coordinated pseudohalide ligands have nonetheless not been available. Previous attempts in our laboratory to synthesize a (μ-oxo)bis(μ-carboxylato)diiron(III) azide complex by self-assembly using monocarboxylates were unsuccessful. In addition, the entire triply bridged core of the coordinatively saturated Hr model compounds $[Fe_2O(OAc)_2(L)_2]^{2+}$, where L = 1,4,7-triazacyclononane and 1,4,7-trimethyl-1,4,7-triazacyclononane, is disassembled by excess azide and thiocyanate to afford the mononuclear complexes $[FeLX_3]$, where $X = N_3^-$ and NCS^-.[13]

In the present work, we have taken advantage of the ability of XDK to stabilize dimetallic structures to generate the neutral (μ-oxo)(μ-XDK)diiron(III) complexes, $[Fe_2O(\mu\text{-XDK})(bpy)_2(NCS)_2]$ (**1**), $[Fe_2O(\mu\text{-XDK})(bpy)_2(NCSe)_2]$ (**2**), and $[Fe_2O(\mu\text{-XDK})(bpy)_2(N_3)_2]$ (**3**), where bpy = 2,2′-bipyridyl. The single-crystal X-ray crystal structures and optical, infrared, resonance Raman, and Mössbauer spectroscopic properties of **1**−**3** are presented. These complexes constitute the first well-characterized synthetic examples of pseudohalide-bound (μ-oxo)bis(μ-carboxylato)diiron(III) compounds, and they reflect the properties exhibited by the corresponding pseudohalide-bound derivatives of metHr.

Experimental Section

General Methods. The compounds H_2XDK[7] and $[Fe_2O(\mu\text{-XDK})(MeOH)_5(H_2O)](NO_3)_2$ (**4**)[4] were synthesized according to literature procedures. Isothiocyanato- and azidometHr were prepared from Hr isolated from *Phascolopsis gouldii* marine worms (Woods Hole Marine Biological Laboratory) as described previously.[14−16] All other reagents were used as received from commercial sources. Isotopically enriched $NaSC^{15}N$ (>98 atom % ^{15}N) and $Na^{15}NNN$ (>98 atom % ^{15}N) were purchased from Cambridge Isotope Laboratories. Elemental analyses were performed on recrystallized material that was powdered and dried under vacuum with moderate heating (<60 °C).

Synthesis of $[Fe_2O(\mu\text{-XDK})(bpy)_2(NCS)_2]$ (1). A solution containing bpy (8.0 mg, 51 μmol) in MeOH (1 mL) was added with stirring to a dark green solution of **4** (26 mg, 26 μmol) in MeOH (2 mL). To the resulting brown solution was added dropwise a solution of NaSCN (4.1 mg, 51 μmol) in MeOH (1 mL), generating a green solution which was subsequently evaporated to dryness under a stream of nitrogen. The solid residue was extracted with CH_2Cl_2 (3 mL) and the resulting solution filtered. The filtrate was layered carefully with benzene, and the mixture was allowed to equilibrate at room temperature. The resulting crystalline precipitate was washed with benzene and dried in air to yield dark green crystals of **1**·$2C_6H_6$ (27 mg, 82%). FTIR (cm^{-1}, KBr pellet): 2962, 2929, 2054 (ν_{CN}), 1732, 1693, 1548, 1443, 1361, 1192, 764, 736. UV−vis (λ_{max}, nm (ϵ, M^{-1} cm^{-1} Fe^{-1}), $CHCl_3$): 405 (5.4×10^3), 642 (1.2×10^2). Anal. Calcd for $C_{54}H_{54}N_8O_9S_2Fe_2$: C, 57.15; H, 4.80; N, 9.87. Found: C, 57.15; H, 4.66; N, 9.95.

Synthesis of $[Fe_2O(\mu\text{-XDK})(bpy)_2(^{15}NCS)_2]$ (1a). Compound **1a** was synthesized according to the procedure described for **1** except that 2 equiv of $NaSC^{15}N$ was employed. FTIR (cm^{-1}, KBr pellet): 2030 ($\nu_{C^{15}N}$).

Synthesis of $[Fe_2O(\mu\text{-XDK})(bpy)_2(NCSe)_2]$ (2). A solution of bpy (21.3 mg, 136 μmol) in MeOH (2 mL) was added dropwise with stirring followed by KSeCN (19.7 mg, 137 μmol) dissolved in MeOH (2 mL) to a solution of **4** (75 mg, 74 μmol) in MeOH (4 mL). This solution was evaporated to dryness, and the resulting red-brown residue was extracted with CH_2Cl_2 (5 mL). The solution was filtered and the filtrate layered with benzene. Upon equilibration at room temperature, a crystalline precipitate formed which was washed with benzene and dried in air to yield dark orange-brown crystals of **2**·$2C_6H_6$ (80.4 mg, 85.4%). FTIR (cm^{-1}, KBr pellet): 2964, 2930, 2054 (ν_{CN}), 1732, 1693, 1543, 1444, 1362, 1192, 764, 736. UV−vis (λ_{max}, nm (ϵ, M^{-1} cm^{-1} Fe^{-1}), $CHCl_3$): 430 (3.7×10^3), 646 (1.4×10^2). Anal. Calcd for $C_{54}H_{54}N_8O_9Se_2Fe_2$: C, 52.79; H, 4.43; N, 9.12. Found: C, 52.46; H, 4.34; N, 9.03.

Synthesis of $[Fe_2O(\mu\text{-XDK})(bpy)_2(N_3)_2]$ (3). Solid bpy (87.2 mg, 558 μmol) followed dropwise by NaN_3 (36.3 mg, 558 μmol) dissolved in MeOH (3 mL) was added with stirring to a solution of **4** (279 mg, 277 μmol) in MeOH (10 mL), during which a red precipitate formed. The reaction mixture was evaporated to dryness and the resulting residue was extracted with CH_2Cl_2 (10 mL). The solution was filtered, and the green-black solid that was removed was further extracted with CH_2Cl_2 in 1-mL portions until all of the colored material was solubilized. The combined solution was layered with toluene and allowed to equilibrate at 4 °C. The resulting black crystalline precipitate was rinsed with toluene and dried in air to yield a dark red-brown powder. The supernatant was evaporated to dryness, and the resulting residue was used for another round of crystallization. This procedure was repeated multiple times for maximal recovery of **3** (299 mg, 97.9%). FTIR (cm^{-1}, KBr pellet): 2965, 2929, 2043 (ν_{as,N_3}), 1731, 1690, 1552, 1444, 1361, 1193, 765, 737. UV−vis (λ_{max}, nm (ϵ, M^{-1} cm^{-1} Fe^{-1}), $CHCl_3$): 425 (2.9×10^3), 648 (1.1×10^2). Anal. Calcd for $C_{52}H_{54}N_{12}O_9Fe_2$: C, 56.64; H, 4.94; N, 15.24. Found: C, 56.90; H, 5.35; N, 14.83.

Synthesis of $[Fe_2O(\mu\text{-XDK})(bpy)_2(^{15}NNN)_2]$ (3a). Compound **3a** was synthesized according to the procedure described for **3** except that 2 equiv of $Na^{15}NNN$ was employed. FTIR (cm^{-1}, KBr pellet): 2035 ($\nu_{as,^{15}NNN}$).

X-ray Crystallography. X-ray quality crystals of **1** and **2** were obtained directly from the synthetic procedures described above whereas those of **3** were obtained from CH_2Cl_2 solutions layered with mesitylene. Crystals were mounted in Paratone N oil on the ends of glass capillaries and frozen into place under a low-temperature nitrogen cold stream. Data were collected on a Siemens SMART/CCD X-ray diffractometer with Mo Kα radiation (λ = 0.710 73 Å). Details of the data collection and reduction protocols are described elsewhere.[5]

The structures were solved by direct methods and refined on F^2 by using the SHELXTL software package. All nonhydrogen atoms were refined anisotropically. Hydrogen atoms were assigned idealized positions and isotropic thermal parameters equivalent to either 1.5 (methyl hydrogens) or 1.2 (all other hydrogens) times the thermal parameter of the carbon atom to which they were attached. Empirical

(8) (a) Hagen, K. S.; Lachicotte, R.; Kitaygorodskiy, A.; Elbouadili, A. *Angew. Chem., Int. Ed. Engl.* **1993**, *32*, 1321−1324. (b) Tanase, T.; Yun, J. W.; Lippard, S. J. *Inorg. Chem.* **1995**, *34*, 4220−4229. (c) Tanase, T.; Lippard, S. J. *Inorg. Chem.* **1995**, *34*, 4682−4690. (d) Yun, J. W.; Tanase, T.; Lippard, S. J. *Inorg. Chem.* **1996**, *35*, 7590−7600. (e) LeCloux, D. D.; Lippard, S. J. *Inorg. Chem.*, in press.
(9) (a) Watton, S. P.; Davis, M. I.; Pence, L. E.; Rebek, J., Jr.; Lippard, S. J. *Inorg. Chim. Acta* **1995**, *235*, 195−204. (b) Tanase, T.; Yun, J. W.; Lippard, S. J. *Inorg. Chem.* **1996**, *35*, 3585−3594.
(10) Stenkamp, R. E. *Chem. Rev.* **1994**, *94*, 715−726.
(11) Ai, J.; Broadwater, J. A.; Loehr, T. M.; Sanders-Loehr, J.; Fox, B. G. *JBIC* **1997**, *2*, 37−45.
(12) Raner, G. M.; Martins, L. J.; Ellis, W. R., Jr. *Biochemistry* **1997**, *36*, 7037−7043.
(13) Wieghardt, K.; Pohl, K.; Ventur, D. *Angew. Chem., Int. Ed. Engl.* **1985**, *24*, 392−393.
(14) (a) Klotz, I. M.; Klotz, T. A.; Fiess, H. A. *Arch. Biochem. Biophys.* **1957**, *68*, 284−299. (b) Keresztes-Nagy, S.; Klotz, I. M. *Biochemistry* **1965**, *4*, 919- 931.
(15) Garbett, K.; Johnson, C. E.; Klotz, I. M.; Okamura, M. Y.; Williams, R. J. P. *Arch. Biochem. Biophys.* **1971**, *142*, 574−583.
(16) Shiemke, A. K.; Loehr, T. M.; Sanders-Loehr, J. *J. Am. Chem. Soc.* **1986**, *108*, 2437−2443.

Table 1. X-ray Crystallographic Information for $[Fe_2O(\mu\text{-XDK})(bpy)_2(NCS)_2]\cdot 2C_6H_6$ (**1**·$2C_6H_6$), $[Fe_2O(\mu\text{-XDK})(bpy)_2(NCSe)_2]\cdot 2C_6H_6$ (**2**·$2C_6H_6$), and $[Fe_2O(\mu\text{-XDK})(bpy)_2(N_3)_2]\cdot CH_2Cl_2\cdot C_6H_3(CH_3)_3$ (**3**·$CH_2Cl_2\cdot C_6H_3(CH_3)_3$)

	1·$2C_6H_6$	**2**·$2C_6H_6$	**3**·$CH_2Cl_2\cdot C_6H_3(CH_3)_3$
formula	$C_{66}H_{66}N_8O_9S_2Fe_2$	$C_{66}H_{66}N_8O_9Se_2Fe_2$	$C_{62}H_{68}N_{12}O_9Cl_2Fe_2$
fw	1291.09	1384.89	1307.88
cryst size, mm	0.5 × 0.4 × 0.3	0.2 × 0.2 × 0.1	0.4 × 0.2 × 0.2
cryst system	monoclinic	monoclinic	triclinic
space group	$P2_1/n$	$C2/c$	$P\bar{1}$
T, °C	−90	−85	−85
a, Å	19.6692(2)	22.6834(3)	12.1645(2)
b, Å	14.3069(1)	14.4315(2)	14.9196(3)
c, Å	22.6502(3)	19.7013(4)	18.0690(3)
α, deg			79.688(1)
β, deg	96.922(1)	97.837(1)	78.611(1)
γ, deg			83.453(1)
V, Å^3	6327.4(1)	6389.1(2)	3152.3(1)
Z	4	4	2
ρ_{calcd}, g cm^{-3}	1.355	1.440	1.378
abs coeff, mm^{-1}	0.588	1.656	0.610
effective transm factor	0.839−1.00	0.856−1.00	0.803−1.00
2θ range, deg	$2.92 \le 2\theta \le 56.56$	$3.36 \le 2\theta \le 56.56$	$2.32 \le 2\theta \le 56.54$
no. of data	15142	7453	13484
no. of params	814	394	784
R^a ($I > 2\sigma(I)$)	0.0443	0.0559	0.0392
wR^{2b} ($I > 2\sigma(I)$)	0.0984	0.1321	0.0999

[a] $R = \sum||F_o| - |F_c||/\sum|F_o|$. [b] $wR^2 = \{\sum[w(F_o^2 - F_c^2)^2]/\sum[w(F_o^2)^2]\}^{1/2}$.

absorption corrections were applied by using the SADABS program. The most disagreeable reflections with delta(F^2)/esd > 10 were omitted (7 reflections for **1**, 0 for **2**, and 3 for **3**) during the final sets of full-matrix least-squares refinements. For **1**·$2C_6H_6$, one of the benzene molecules was modeled over two half-occupied positions using idealized bond distance and angles. Relevant crystallographic information is summarized in Table 1.

Spectroscopy. Optical spectra were recorded on a Varian Cary 1E spectrophotometer. FT-IR spectra were recorded on a Bio-Rad FTS 135 spectrometer; samples were prepared by pressing into KBr pellets powdered material derived from crystals grown by layer diffusion of benzene into CH_2Cl_2 solutions of the compound. Resonance Raman (RR) spectra were recorded at room temperature using an excitation wavelength of 406.7 nm from a Kr ion laser. Samples were placed in NMR tubes with concentrations ~1 mM in $CHCl_3$. Raman shifts were referenced to known band positions of $CHCl_3$. Mössbauer spectra were recorded at 77 K with a ^{57}Co source in a Rh matrix at room temperature and fit to Lorentzian line shapes. Samples were prepared by suspending powdered material derived from X-ray-quality crystals in Apiezon N grease; isomer shifts were referenced to natural abundance Fe at room temperature.

Results and Discussion

Synthesis. Since the first reports of synthetic (μ-oxo)bis(μ-carboxylato)diiron(III) compounds,[17] numerous others that model the N_3O_3 coordination environment around the iron(III) centers of azidometHr have been described.[18,19] Although these complexes also mimic certain spectroscopic and magnetic properties of azidometHr, the remaining coordination sites around the (μ-oxo)bis(μ-carboxylato)diiron(III) core are generally occupied by either imine or amine N-atom-donor ligands. The structural characterization of an azide-containing (μ-oxo)-bis(μ-carboxylato)diiron(III) complex $[Fe_2O(\mu\text{-OBz})_2(bpy)_2(N_3)_2]$ was mentioned in the literature,[20] but neither this result nor any other characterization of the complex has been published.

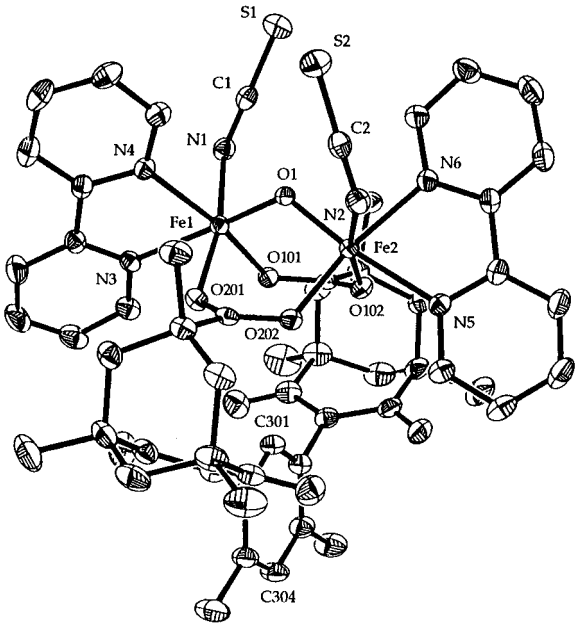

Figure 1. ORTEP diagram of the ΛΛ-isomer of $[Fe_2O(\mu\text{-XDK})(bpy)_2(NCS)_2]$ (**1**) showing 40% probability thermal ellipsoids for all nonhydrogen atoms.

By starting with an effectively coordinatively unsaturated complex containing a preformed triply bridged $\{Fe_2O(\mu\text{-XDK})\}^{2+}$ unit,[4] we were able to synthesize in a facile and efficient manner (μ-oxo)bis(μ-carboxylato)diiron(III) complexes which not only have biomimetic N_3O_3 coordination environments but also contain pseudohalide terminal ligands. Addition of 2 equiv of the bidentate bpy ligand to **4** in methanol generates in situ the brown $[Fe_2O(\mu\text{-XDK})(bpy)_2(MeOH)_2]^{2+}$ cation.[4] The remaining two MeOH ligands are readily replaced by 2 equiv of a pseudohalide to yield the neutral bis(pseudohalide) complexes $[Fe_2O(\mu\text{-XDK})(bpy)_2(NCS)_2]$ (**1**), $[Fe_2O(\mu\text{-XDK})(bpy)_2(NCSe)_2]$ (**2**), and $[Fe_2O(\mu\text{-XDK})(bpy)_2(N_3)_2]$ (**3**).

X-ray Crystal Structures. Complex **1** crystallizes with two molecules of benzene in the lattice. Figure 1 indicates that a

(17) (a) Armstrong, W. H.; Lippard, S. J. *J. Am. Chem. Soc.* **1983**, *105*, 4837−4838. (b) Wieghardt, K.; Pohl, K.; Gebert, W. *Angew. Chem., Int. Ed. Engl.* **1983**, *22*, 727.
(18) Kurtz, D. M., Jr. *Chem. Rev.* **1990**, *90*, 585−606.
(19) For a very recent example, which involves the use of a dinucleating hexapyridine ligand, see: Kodera, M.; Shimakoshi, H.; Nishimura, M.; Okawa, H.; Iijima, S.; Kano, K. *Inorg. Chem.* **1996**, *35*, 4967−4973.
(20) Vincent, J. B.; Huffman, J. C.; Christou, G.; Li, Q.; Nanny, M. A.; Hendrickson, D. N.; Fong, R. H.; Fish, R. H. *J. Am. Chem. Soc.* **1988**, *110*, 6898−6900.

Table 2. Selected Bond Distances (Å) and Angles (deg) for $[Fe_2O(\mu\text{-XDK})(bpy)_2(NCS)_2]\cdot 2C_6H_6$ (**1**·$2C_6H_6$)[a,b]

Bond Distances			
Fe1−O1	1.7907(13)	Fe2−O1	1.7866(13)
Fe1−O101	2.0037(13)	Fe2−O102	2.0937(14)
Fe1−O201	2.0842(14)	Fe2−O202	2.0185(14)
Fe1−N1	2.107(2)	Fe2−N2	2.119(2)
Fe1−N3	2.180(2)	Fe2−N5	2.170(2)
Fe1−N4	2.141(2)	Fe2−N6	2.151(2)
N1−C1	1.166(3)	N2−C2	1.168(3)
C1−S1	1.618(2)	C2−S2	1.621(2)

Bond Angles			
Fe1−O1−Fe2	123.62(7)	Fe2−N2−C2	131.7(2)
Fe1−N1−C1	130.6(2)	O1−Fe2−O102	91.89(6)
O1−Fe1−O101	98.96(6)	O1−Fe2−O202	98.26(6)
O1−Fe1−O201	91.82(6)	O1−Fe2−N2	95.59(7)
O1−Fe1−N1	94.67(7)	O1−Fe2−N5	167.58(7)
O1−Fe1−N3	165.91(6)	O1−Fe2−N6	95.38(6)
O1−Fe1−N4	95.18(6)	N2−Fe2−O102	168.32(6)
N1−Fe1−O101	89.82(6)	N2−Fe2−O202	87.34(6)
N1−Fe1−O201	169.77(6)	N2−Fe2−N5	91.25(7)
N1−Fe1−N3	94.59(7)	N2−Fe2−N6	82.28(7)
N1−Fe1−N4	85.70(7)	N5−Fe2−O102	79.84(6)
N3−Fe1−O101	91.66(6)	N5−Fe2−O202	92.39(6)
N3−Fe1−O201	77.64(6)	N5−Fe2−N6	75.25(6)
N3−Fe1−N4	74.96(6)	N6−Fe2−O102	88.12(6)
N4−Fe1−O101	165.47(6)	N6−Fe2−O202	163.59(6)
N4−Fe1−O201	85.84(6)	O102−Fe2−O202	100.47(6)
O101−Fe1−O201	96.99(6)	N2−C2−S2	179.2(2)
N1−C1−S1	178.8(2)		

Torsion Angles[c]			
N1−C1−Fe1−O1	−19.0	N2−C2−Fe2−O1	−18.9

[a] See Figure 1 for the atom-labeling scheme. [b] Numbers in parentheses are estimated standard deviations for the last significant digit. [c] The torsion angle J−I−K−L is defined as the angle between the bond vectors J−I and K−L when viewed down the J−K bond in ΛΛ-$[Fe_2O(\mu\text{-XDK})(bpy)_2(NCS)_2]$. The value is positive if J−I is rotated clockwise into K−L and negative if J−I is rotated counterclockwise into K−L.

noncrystallographic C_2 axis passes through O1, C301, and C304, relating the two halves of the molecule. Selected bond distance and angles are listed in Table 2. As anticipated from previous work,[4] the two iron centers are displaced from the plane of the XDK bridging carboxylate ligands, and a third bridge is provided by an oxo group. The Fe−O−Fe angle of 123.62(7)° and the average $Fe-O_{oxo}$ bond distance of 1.789(2) Å are nearly identical to values reported in other crystallographically characterized (μ-oxo)(μ-XDK)diiron(III) complexes.[4] The distorted octahedral coordination geometry around each iron atom is completed by a bidentate bpy and a terminal SCN^- ligand that is N-bonded, consistent with the relatively hard nature of the formally Fe(III) centers in the $\{Fe_2O(\mu\text{-XDK})(bpy)_2\}^{2+}$ unit. The two bpy ligands are oriented anti with respect to the $Fe-O_{oxo}-Fe$ plane, rendering **1** chiral. The bound isothiocyanate ligands are linear and coordinated cis to the oxo group. The Fe−N−C angles are bent, averaging 131.2(6)°. The $N-C-Fe-O_{oxo}$ torsion angles are −18.9 and −19.0°, respectively, for the two halves of the molecule.

X-ray quality crystals of **2** were grown in an identical fashion. The structure is depicted in Figure 2, and selected bond distances and angles are listed in Table 3. As in **1**·$2C_6H_6$, two molecules of benzene are found for every molecule of **2** in the crystal. Unlike **1**, however, a true crystallographic C_2 axis relates the two halves of **2**. Compounds **1**·$2C_6H_6$ and **2**·$2C_6H_6$ are nearly but not rigorously isomorphous, although the metal complexes are nonetheless isostructural. In particular, the Fe−N−C angle of 129.7(3)° and the $N-C-Fe-O_{oxo}$ torsion angle of −20.6° indicate that the isoselenocyanate ligand is in essentially the same orientation as observed for the isothiocyanate ligands in **1**·$2C_6H_6$.

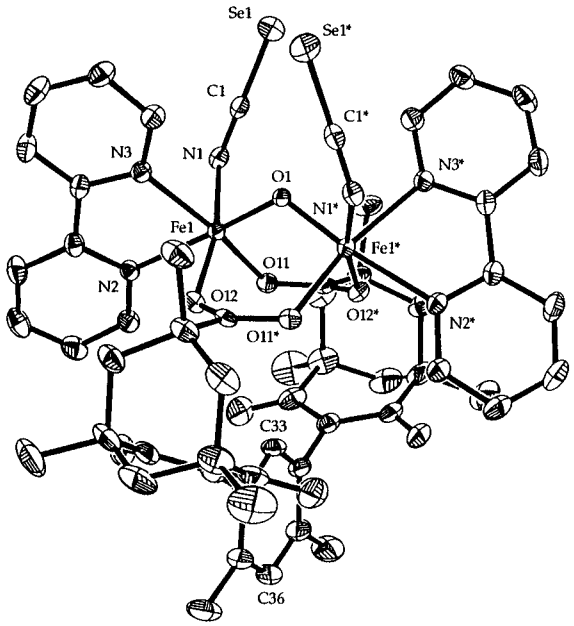

Figure 2. ORTEP diagram of the ΛΛ-isomer of $[Fe_2O(\mu\text{-XDK})(bpy)_2(NCSe)_2]$ (**2**) showing 40% probability thermal ellipsoids for all nonhydrogen atoms. Labels with asterisks refer to symmetry-generated atoms. A crystallographic 2-fold rotation axis passes through O1, C33, and C36.

Table 3. Selected Bond Distances (Å) and Angles (deg) for $[Fe_2O(\mu\text{-XDK})(bpy)_2(NCSe)_2]\cdot 2C_6H_6$ (**2**·$2C_6H_6$)[a,b]

Bond Distances			
Fe1−O1	1.787(2)	Fe1−N2	2.174(3)
Fe1−O11	2.011(2)	Fe1−N3	2.140(3)
Fe1−O12	2.078(2)	N1−C1	1.167(5)
Fe1−N1	2.132(3)	C1−Se1	1.776(4)

Bond Angles			
Fe1−O1−Fe1*	123.3(2)	N1−Fe1−N2	92.62(11)
Fe1−N1−C1	129.7(3)	N1−Fe1−N3	83.13(11)
O1−Fe1−O11	98.39(9)	N2−Fe1−O11	91.44(10)
O1−Fe1−O12	92.00(9)	N2−Fe1−O12	79.31(10)
O1−Fe1−N1	94.77(11)	N2−Fe1−N3	75.09(11)
O1−Fe1−N2	167.89(8)	N3−Fe1−O11	163.41(10)
O1−Fe1−N3	96.28(10)	N3−Fe1−O12	87.45(10)
N1−Fe1−O11	87.96(11)	O11−Fe1−O12	99.71(10)
N1−Fe1−O12	168.93(10)	N1−C1−Se1	178.0(3)

Torsion Angle[c]	
N1−C1−Fe1−O1	−20.6

[a] See Figure 2 for the atom-labeling scheme. [b] Numbers in parentheses are estimated standard deviations for the last significant digit. [c] The torsion angle J−I−K−L is defined as the angle between the bond vectors J−I and K−L when viewed down the J−K bond in ΛΛ-$[Fe_2O(\mu\text{-XDK})(bpy)_2(NCSe)_2]$. The value is positive if J−I is rotated clockwise into K−L and negative if J−I is rotated counterclockwise into K−L.

Structural differences between **1** and **2** are limited to the carbon-chalcogen bond distances, averaging 1.620(2) and 1.776(4) Å, respectively. This result reflects the smaller covalent radius of sulfur (1.02 Å) compared to selenium (1.17 Å).[21] Furthermore, a comparison between a crystallographically characterized copper(II) complex with coordinated isothiocyanate ligands, [Cu(2,2′:6′,2″-terpyridine)$(NCS)_2$],[22] and one in which the isothiocyanates are replaced by isoselenocyanates,

(21) Huheey, J. E.; Keiter, E. A.; Keiter, R. L. *Inorganic Chemistry: Principles of Structure and Reactivity*, 4th ed.; HarperCollins: New York, 1993; Chapter 8, pp 291−296.

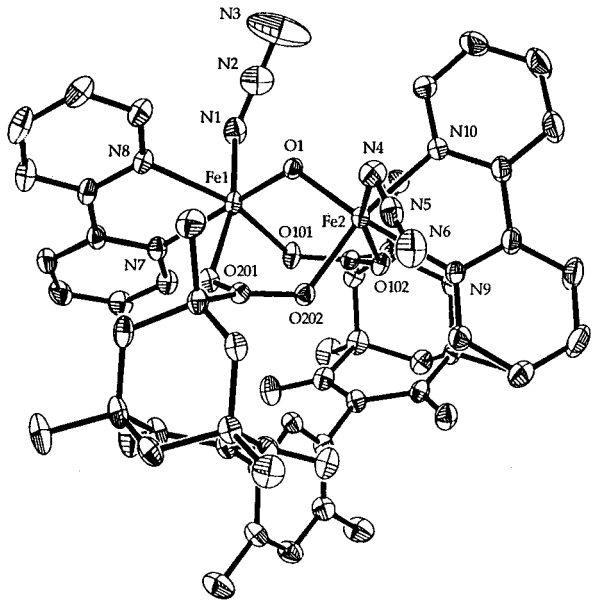

Figure 3. ORTEP diagram of the ΛΛ-isomer of $[Fe_2O(\mu\text{-XDK})(bpy)_2(N_3)_2]$ (**3**) showing 40% probability thermal ellipsoids for all nonhydrogen atoms.

$[Cu(2,2'{:}6',2''\text{-terpyridine})(NCSe)_2]$,[23] shows the same difference in carbon−chalcogen bond distances: 1.631(8) and 1.75(3) Å, respectively. Although there are numerous examples of iron(III)−isothiocyanate complexes in the Cambridge Structural Database, **2** constitutes the first example of a structurally characterized (isoselenocyanato)iron(III) complex.

The conditions employed to generate X-ray quality specimens of **1** and **2** yielded only irregularly shaped crystals of the bis(azido) complex **3**. Substitution of mesitylene for benzene as the precipitant, however, afforded crystals suitable for X-ray crystallography. Figure 3 shows the structure of **3**, and Table 4 lists selected bond distances and angles. The metrical parameters of the (μ-oxo)(μ-XDK)bis(bpy)diiron(III) portion of **3** are very similar to those observed in **1** and **2**. A major difference, however, is the relative orientation of the two linear azide ligands. In **3**, the two halves of the molecule are not related by the C_2 symmetry axis found in the structures of **1** and **2**. The N1−N2−Fe1−O1 torsion angle is −14.7° whereas that for N4−N5−Fe2−O1 is +146.4°. Additional asymmetry is observed in the small but significant differences in the Fe−N bond lengths and Fe−N−N angles, as well as in the intraligand N−N bond distances. The near linearity of the N−N−N angles and the N−N bond lengths are typical of coordinated azide ions.[24]

When crystals of **3** were grown by layer diffusion of toluene into a CH_2Cl_2 solution at 33 °C, the resulting structure had C_2 symmetry and N1−N2−Fe1−O1 torsion angles of ∼−23°.[25] Thus, in the solid state, there appears to be a preference for pseudohalide ligands bound to the $\{Fe_2O(\mu\text{-XDK})(bpy)_2\}^{2+}$ unit to adopt a conformation such that the (pseudohalide)−(iron−oxo) torsion angle is ∼−20°. Although this eclipsed orientation may indicate an electronic bias, the difference in stability between the two disparate azide conformations observed in **3**·CH_2Cl_2·$C_6H_3(CH_3)_3$ is small enough to be overcome by crystal packing forces. There are no steric interactions that would appear to preclude rotation about the iron-pseudohalide bonds in **1**−**3** in solution. The barrier for this process, however, and whether the eclipsed and trans conformations might represent local minima in energy have not been determined.

Table 4. Selected Bond Distances (Å) and Angles (deg) for $[Fe_2O(\mu\text{-XDK})(bpy)_2(N_3)_2]$·$CH_2Cl_2$·$C_6H_3(CH_3)_3$ (**3**·CH_2Cl_2·$C_6H_3(CH_3)_3$)[a,b]

Bond Distances			
Fe1−O1	1.8049(14)	Fe2−O1	1.8023(13)
Fe1−O101	2.0430(14)	Fe2−O102	2.1123(14)
Fe1−O201	2.1635(14)	Fe2−O202	2.0103(14)
Fe1−N1	2.050(2)	Fe2−N4	2.081(2)
Fe1−N7	2.184(2)	Fe2−N9	2.206(2)
Fe1−N8	2.173(2)	Fe2−N10	2.162(2)
N1−N2	1.160(3)	N4−N5	1.194(3)
N2−N3	1.152(4)	N5−N6	1.165(3)

Bond Angles			
Fe1−O1−Fe2	123.74(8)	Fe2−N4−N5	119.1(2)
Fe1−N1−N2	124.1(2)	O1−Fe2−O102	94.37(6)
O1−Fe1−O101	99.50(6)	O1−Fe2−O202	97.53(6)
O1−Fe1−O201	89.76(6)	O1−Fe2−N4	102.35(7)
O1−Fe1−N1	97.76(7)	O1−Fe2−N9	167.17(6)
O1−Fe1−N7	171.10(6)	O1−Fe2−N10	96.10(6)
O1−Fe1−N8	100.55(6)	N4−Fe2−O102	161.51(7)
N1−Fe1−O101	89.74(7)	N4−Fe2−O202	89.86(7)
N1−Fe1−O201	167.97(7)	N4−Fe2−N9	86.45(7)
N1−Fe1−N7	89.43(7)	N4−Fe2−N10	86.80(7)
N1−Fe1−N8	89.12(7)	N9−Fe2−O102	75.81(6)
N7−Fe1−O101	85.72(6)	N9−Fe2−O202	91.75(6)
N7−Fe1−O201	82.31(6)	N9−Fe2−N10	74.86(6)
N7−Fe1−N8	74.19(7)	N10−Fe2−O102	83.57(6)
N8−Fe1−O101	159.89(6)	N10−Fe2−O202	166.36(6)
N8−Fe1−O201	80.24(6)	O102−Fe2−O202	95.80(6)
O101−Fe1−O201	98.31(6)	N4−N5−N6	177.3(2)
N1−N2−N3	176.8(3)		

Torsion Angles[c]			
N1−N2−Fe1−O1	−14.7	N4−N5−Fe2−O1	+146.4

[a] See Figure 3 for the atom-labeling scheme. [b] Numbers in parentheses are estimated standard deviations for the last significant digit. [c] The torsion angle J−I−K−L is defined as the angle between the bond vectors J−I and K−L when viewed down the J−K bond in ΛΛ-$[Fe_2O(\mu\text{-XDK})(bpy)_2(N_3)_2]$ The value is positive if J−I is rotated clockwise into K−L and negative if J−I is rotated counterclockwise into K−L.

The average N−N−Fe−O_{oxo} torsion angle in azidometHr is −3.6° (esd 6.2°) for the four independent molecules in the crystal structure.[26] Therefore, the geometry at Fe1 in **3**·CH_2Cl_2·$C_6H_3(CH_3)_3$ most closely resembles the azide-bearing iron center in azidometHr. The shape of the active-site cavity of Hr[27] presumably restricts the motion of coordinated azide in the azidomet derivative. Apart from the hydrophobic nature of the active site,[16] a reduction in available conformational space of a bound ligand could be important for the protein to function as a reversible dioxygen carrier. The bound hydroperoxide in oxyHr may be stabilized by orienting the O−O bond such that the O−O−Fe−O_{oxo} torsion angle adopts the eclipsed conformation, positioning the hydroperoxide proton to form the putative hydrogen bond with the oxo bridge.[16]

Electronic Spectroscopy. The optical spectra of compounds **1**−**3** display relatively intense absorptions between 350 and 550 nm as well as weaker bands centered ∼650 nm (Figure 4). The positions and intensities of the lower energy bands fall in the

(22) Arriortua, M. I.; Mesa, J. L.; Rojo, T.; Debaerdemaeker, T.; Beltrán-Porter, D.; Stratemeier, H.; Reinen, D. *Inorg. Chem.* **1988**, *27*, 2976−2981.
(23) Rojo, T.; Garcia, A.; Mesa, J. L.; Via, J.; Arriortua, M. I. *Inorg. Chim. Acta* **1988**, *149*, 159−161.
(24) Dori, Z.; Ziolo, R. F. *Chem. Rev.* **1973**, *73*, 247−254.
(25) A complete structure determination was hampered by severe disorder in lattice solvent molecules. Crystal data: monoclinic, *P*2/*n*, a = 14.3159(2) Å, b = 13.5970(4) Å, c = 19.4417(3) Å, β = 110.936(1)°, Z = 2, T = −85 °C.
(26) Holmes, M. A.; Stenkamp, R. E. *J. Mol. Biol.* **1991**, *220*, 723−737.
(27) Stenkamp, R. E.; Sieker, L. C.; Jensen, L. H.; McCallum, J. D.; Sanders-Loehr, J. *Proc. Natl. Acad. Sci. U.S.A.* **1985**, *82*, 713−716.

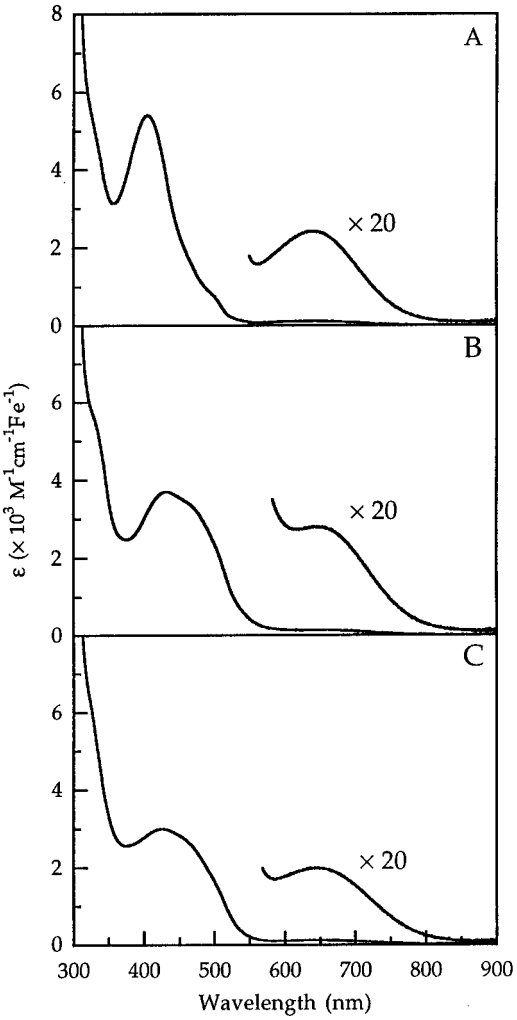

Figure 4. Electronic absorption spectra of (A) $[Fe_2O(\mu\text{-XDK})(bpy)_2(NCS)_2]$ (**1**), (B) $[Fe_2O(\mu\text{-XDK})(bpy)_2(NCSe)_2]$ (**2**), and (C) $[Fe_2O(\mu\text{-XDK})(bpy)_2(N_3)_2]$ (**3**) in $CHCl_3$.

range observed in other (μ-oxo)bis(μ-carboxylato)diiron(III) complexes.[18] This set of absorption bands arises from the $^6A_1 \rightarrow [^4T_2]$(^{4}G) transition of high-spin iron(III) in an octahedral coordination environment.[28] The absorption maxima of this band in **1**−**3** are very close to one another, implying that the iron centers in these complexes occupy very similar ligand-field environments. These transitions are, however, blue-shifted considerably from the corresponding ones in isothiocyanato- and azidometHr.[29] This difference indicates that the ligand-field strength experienced by the iron centers in the protein systems is *greater* than in the model compounds,[28] consistent with the stronger ligand field induced by polyimidazole versus polypyridine coordination.[3]

The absorptivity of **1**−**3** in the 350−550-nm range is much greater than is observed for previously reported synthetic (μ-oxo)bis(μ-carboxylato)diiron(III) complexes.[18] The increased intensity in this wavelength region is attributed to pseudohalide-to-iron(III) charge-transfer transitions which overlap with the weaker high-energy ligand-field transitions.[28] Solutions of **2** and **3** are both red and exhibit very similar absorption profiles, suggesting that the iron centers in **2** and **3** possess similar electronic structures. The iron centers in **1**, however, can be considered electronically distinct from those of **2** and **3** because solutions of **1** are green and show a much sharper band shape in the pseudohalide-to-iron(III) charge-transfer region.

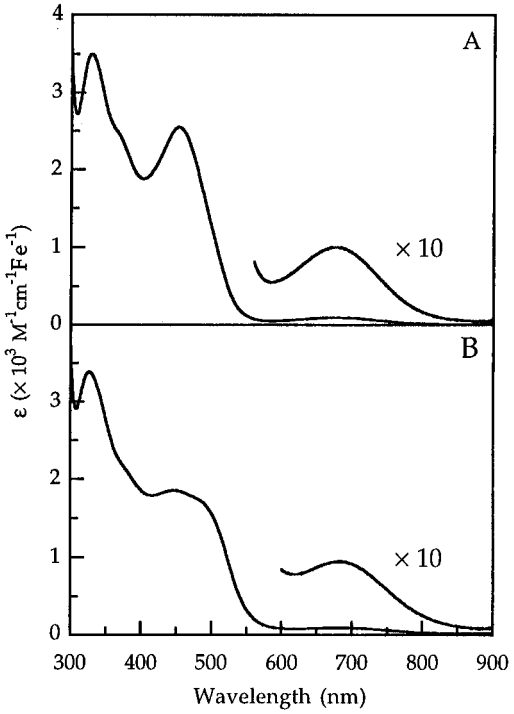

Figure 5. Electronic absorption spectra of (A) isothiocyanatometHr in 0.1 M Tris-SO_4/0.1 M NaSCN (pH 8.0) and (B) azidometHr in 0.1 M Tris-SO_4/0.015 M NaN_3 (pH 8.0).

Although blue-shifted, the shapes and intensities of the absorption bands observed in bis(isothiocyanate) **1** and bis(azide) **3** bear a striking resemblance to those of the corresponding isothiocyanate- and azide-bound derivatives of metHr[29] (Figure 5). The molar absorptivities of the higher energy bands between the model and protein systems match very closely after correcting for the presence of two pseudohalide ligands per diiron center in **1** and **3** as opposed to only one in the protein. By taking the contribution from ligand-field transitions to be ~400 M^{-1} cm^{-1} Fe^{-1} at λ_{max} of the higher energy bands,[4] the extinction coefficients at λ_{max} are estimated to be 2900 M^{-1} cm^{-1} Fe^{-1} for **1**, compared to 2550 M^{-1} cm^{-1} Fe^{-1} for isothiocyanatometHr, and 1650 M^{-1} cm^{-1} Fe^{-1} for **3**, compared to 1850 M^{-1} cm^{-1} Fe^{-1} for azidometHr.

Vibrational Spectroscopy. Compounds **1**−**3** exhibit very strong IR bands ~2050 cm^{-1}, characteristic of terminally coordinated isothiocyanate, isoselenocyanate, and azide moieties.[30] The CN stretching frequencies of the isothiocyanate and isoselenocyanate ligands in **1** and **2**, respectively, both occur at 2054 cm^{-1}. This result is not surprising considering the identical pseudohalide C−N bond distances for **1** and **2**. The isothiocyanate CN stretching frequency shifts to 2030 cm^{-1} in **1a**, consistent with an increase in the reduced mass of the CN oscillator upon ^{15}N substitution. Nevertheless, the observed shift is 8 cm^{-1} less than the value predicted from a diatomic harmonic oscillator model, indicating that the CN stretch is coupled to other vibrational modes. The corresponding CN stretching frequency in isothiocyanatometHr was measured by RR spectroscopy to be 2043 cm^{-1}.[31] This frequency occurs at 2017

(28) Reem, R. C.; McCormick, J. M.; Richardson, D. E.; Devlin, F. J.; Stephens, P. J.; Musselman, R. L.; Solomon, E. I. *J. Am. Chem. Soc.* **1989**, *111*, 4688−4704.
(29) Garbett, K.; Darnall, D. W.; Koltz, I. M.; Williams, R. J. P. *Arch. Biochem. Biophys.* **1969**, *135*, 419−434.
(30) Nakamoto, K. *Infrared Spectra of Inorganic and Coordination Compounds*, 2nd ed.; Wiley Interscience: New York, 1970; Section III-6, pp 187−190.
(31) Kurtz, D. M., Jr.; Shriver, D. F.; Klotz, I. M. *Coord. Chem. Rev.* **1977**, *24*, 145−178.

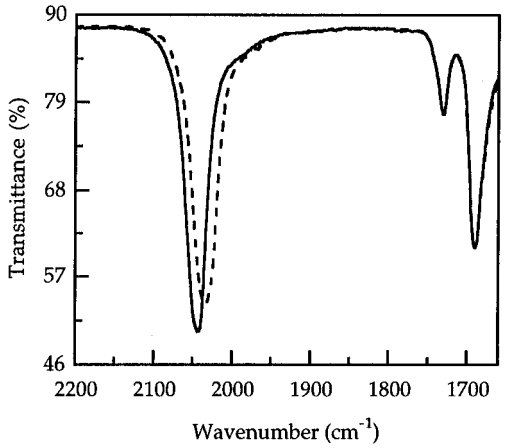

Figure 6. Overlay of the IR spectra (KBr pellet) of $[Fe_2O(\mu\text{-XDK})(bpy)_2(N_3)_2]$ (**3**) (—) and $[Fe_2O(\mu\text{-XDK})(bpy)_2(^{15}NNN)_2]$ (**3a**) (- - -).

cm^{-1} in the ^{15}N-labeled isothiocyanate sample,[31] a shift 6 cm^{-1} less than that predicted for a pure CN oscillator.

The asymmetric azide stretch of **3** occurs at 2043 cm^{-1} and shifts to an apparent single band at 2035 cm^{-1} upon substitution with $^{15}NNN^-$ in **3a** (Figure 6). The corresponding mode in azidometHr appears as a much sharper RR band at 2050 cm^{-1}.[31] The use of $^{15}NNN^-$ in the azidometHr system not only shifts the position of this stretch to lower energy but also splits it into two peaks, at 2032 and 2044 cm^{-1}, reflecting the two possible isotope linkage isomers of a terminally bound $^{15}NNN^-$ ligand.[31] The bands arising from the ^{14}N-bound and ^{15}N-bound azide ligands in the model complex **3a** are presumably too broad and close in energy to be resolved, but an indication of the presence of isotope linkage isomers is the slightly greater breadth of the 2035-cm^{-1} band in **3a** (fwhm = 37 cm^{-1}) compared to the 2043-cm^{-1} band in **3** (fwhm = 31 cm^{-1}).

The RR spectrum of the azide adduct of the (μ-oxo)bis(μ-carboxylato)diiron(III) core of Δ9D at pH 6.2 is dominated by a band at 2100 cm^{-1} that is also considerably broader than the one seen for azidometHr.[11] This band shifts to a broad, single peak at 2089 cm^{-1} upon substitution with $^{15}NNN^-$.[11] The presence of only a single, asymmetric azide stretching band in the $^{15}NNN^-$ adduct of Δ9D was used to exclude an azidometHr-like active-site structure containing a terminally bound azide. Instead, a novel structure in which the diiron(III) center is bridged symmetrically by azide in a μ-1,3 coordination mode was proposed.[11] Although the absolute frequencies of the bands in the Δ9D system are significantly higher than those in our bis(azide) model complexes, the IR properties of **3a** clearly indicate that the occurrence of only one asymmetric $^{15}NNN^-$ stretch is not sufficient to discount the possibility of a terminally bound azide ligand.

The solution-phase RR spectrum of **1** revealed a prominent feature at 520 cm^{-1} upon excitation into the predominantly isothiocyanate-to-iron(III) charge-transfer band using 406.7-nm light (Figure 7). By analogy to previously studied (μ-oxo)-diiron(III) complexes, this band is assigned to the symmetric stretch of the FeOFe unit. The position of the band is consistent with the 123.62(7)° Fe−O−Fe angle determined for **1**·$2C_6H_6$.[32] Under the same conditions, **2** and **3** showed much weaker RR bands at 520 and 518 cm^{-1}, respectively. The relatively poor resonance enhancement of the symmetric FeOFe stretches in **2** and **3** is ascribed to differences in the electronic absorption profiles of **1**−**3** in the 406.7-nm region (vide supra).

(32) Sanders-Loehr, J.; Wheeler, W. D.; Shiemke, A. K.; Averill, B. A.; Loehr, T. M. *J. Am. Chem. Soc.* **1989**, *111*, 8084−8093.

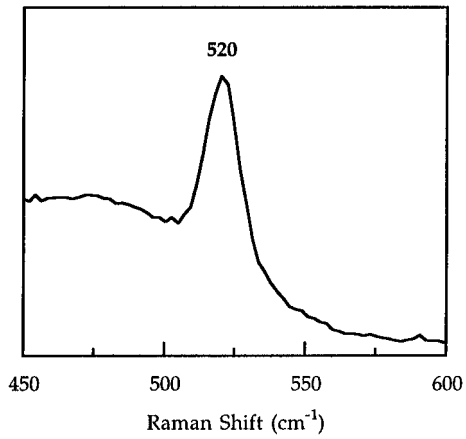

Figure 7. Resonance Raman spectrum of $[Fe_2O(\mu\text{-XDK})(bpy)_2(NCS)_2]$ (**1**) in $CHCl_3$. The sample was excited at 406.7 nm.

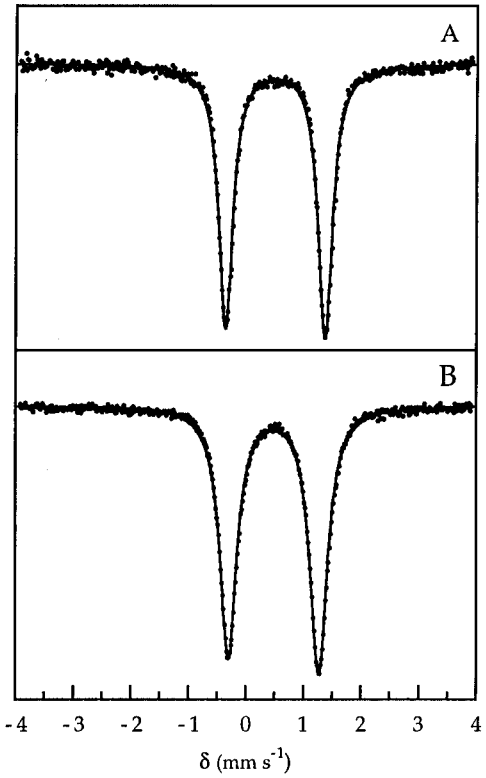

Figure 8. Mössbauer spectra (experimental data (•), calculated fit (—)) of $[Fe_2O(\mu\text{-XDK})(bpy)_2(NCS)_2]$ (**1**) (A) and $[Fe_2O(\mu\text{-XDK})(bpy)_2(N_3)_2]$ (**3**) (B) recorded at 77 K.

Mössbauer Spectroscopy. The Mössbauer spectrum of **1** displays a symmetric quadrupole doublet with $\delta = 0.51$ and $\Delta E_Q = 1.73$ mm s^{-1} (Figure 8A). These values are typical for (μ-oxo)diiron(III) complexes and compare favorably with those of isothiocyanatometHr.[15] Within experimental error, the isomer shift and quadrupole splitting for **2** are identical to those of **1**. The Mössbauer spectrum of **3** is also a symmetric quadrupole doublet exhibiting a nearly identical isomer shift of 0.49 mm s^{-1} (Figure 8B). But the quadrupole splitting of 1.57 mm s^{-1} for **3** is significantly smaller compared to those of **1** and **2**. This difference may be associated with the slightly longer $Fe-O_{oxo}$ bond distances in **3**·CH_2Cl_2·$C_6H_3(CH_3)_3$ compared to those in **1**·$2C_6H_6$ and **2**·$2C_6H_6$, since the magnitude of the quadrupole splitting among triply-bridged (μ-oxo)bis(μ-carboxylato)diiron-(III) complexes tends to decrease as the length of the iron−oxo bonds increases.[18]

Spectroscopic data for **1**−**3**, isothiocyanatoHr, and azidometHr are compiled in Table 5.

Table 5. Spectroscopic Data for $[Fe_2O(\mu\text{-XDK})(bpy)_2(NCS)_2]$ (**1**), $[Fe_2O(\mu\text{-XDK})(bpy)_2(NCSe)_2]$ (**2**), $[Fe_2O(\mu\text{-XDK})(bpy)_2(N_3)_2]$ (**3**), IsothiocyanatometHr (NCSHr), and AzidometHr (N_3Hr)

parameter	**1**	**2**	**3**	NCSHr	N_3Hr
optical spectroscopy					
λ_{max}, nm (ϵ, M^{-1} cm^{-1} Fe^{-1})	405 (5400)	430 (3700)	425 (2900)	452 (2550)[a]	446 (1850)[a]
	642 (120)	646 (140)	648 (110)	674 (100)[a]	680 (95)[a]
vibrational spectroscopy					
ν_{CN}, cm^{-1}	2054	2054		2043[b]	
$\nu_{C^{15}N}$, cm^{-1}	2030			2017[b]	
ν_{as,N_3}, cm^{-1}			2043		2050[b]
$\nu_{as,^{15}NNN}$, cm^{-1}			2035		2032, 2044[b]
$\nu_{s,FeOFe}$, cm^{-1}	520	520	518	511[b]	507[b]
Mössbauer spectroscopy (77 K)					
δ, mm s^{-1}	0.51	0.51	0.49	0.55[c]	0.50[c]
ΔE_Q, mm s^{-1}	1.73	1.75	1.57	1.92[c]	1.91[c]

[a] Reference 29. [b] Reference 31. [c] Reference 15.

Conclusion

Pseudohalide-containing (μ-oxo)bis(μ-carboxylato)diiron(III) compounds have been synthesized. The iron centers of **1**−**3** possess distorted octahedral geometries in which the pseudohalide ligands are N-bound in a terminal bonding mode cis to the oxo bridge. The ligands are anti to one another across the Fe−O−Fe plane. The X-ray structures of **1** and **2** are C_2 symmetric and nearly isostructural, whereas that of **3** (in **3**·CH_2Cl_2·$C_6H_3(CH_3)_3$) is distinguished by conformational asymmetry in the azide ligands. The spectroscopic properties of **1**−**3** (Table 5) are fully consistent with their respective solid-state structures. Compounds **1** and **2** are practically indistinguishable by IR and Mössbauer spectroscopy, whereas **2** and **3** behave more alike when examined by UV−vis and RR spectroscopy. Compound **3a** demonstrates that the two asymmetric azide stretching frequencies arising from linkage isomers of a terminally bound $^{15}NNN^-$ ligand may not necessarily be resolved, urging caution in the interpretation of analogous data for the active sites of carboxylate-bridged diiron proteins. Finally, compounds **1** and **3** reproduce both structural and spectroscopic aspects of isothiocyanato- and azidometHr, respectively.

Acknowledgment. This work was supported by grants from the National Science Foundation and the National Institute of General Medical Sciences. T.J.M. acknowledges the National Institute of Allergies and Infectious Diseases for a postdoctoral fellowship. We thank Prof. William M. Reiff of Northeastern University and Dr. Maria T. Bautista for assistance in obtaining the Mössbauer and RR spectra, respectively, and Dr. Bautista for helpful comments.

Supporting Information Available: Complete listings of crystallographic data, atomic coordinates, bond lengths and angles, and anisotropic displacement parameters (Tables S1−S15) and atom-labeling schemes (Figures S1−S3) for **1**−**3** (36 pages). Ordering information is given on any current masthead page.

IC970397G